

Design of an optically-transparent ultra-broadband microwave absorber

Mian Gao(高冕), Qiang Chen(陈强), Yue-Jun Zheng(郑月军), Fang Yuan(袁方), Zhan-Shan Sun(孙占山), and Yun-Qi Fu(付云起)

Citation: Chin. Phys. B, 2023, 32 (**8**): 084102. DOI: 10.1088/1674-1056/ac9a39
Journal homepage: http://cpb.iphy.ac.cn; http://iopscience.iop.org/cpb

What follows is a list of articles you may be interested in

A novel power-combination method using a time-reversal pulse-compression technique

Xi-Cheng Lu(陆希成), Jin Tian(田锦), Rong-Wei Zhang(张荣威), Hai-Bo Wang(汪海波), and Yang Qiu(邱扬)
Chin. Phys. B, 2023, 32 (**8**): 084101. DOI: 10.1088/1674-1056/acaa2a

High gain and circularly polarized substrate integrated waveguide cavity antenna array based on metasurface

Hao Bai(白昊), Guang-Ming Wang(王光明), and Xiao-Jun Zou(邹晓鋆)
Chin. Phys. B, 2023, 32 (**1**): 014101. DOI: 10.1088/1674-1056/ac6b22

Design method of reusable reciprocal invisibility and phantom device

Cheng-Fu Yang(杨成福), Li-Jun Yun(云利军), and Jun-Wei Li(李俊玮)
Chin. Phys. B, 2022, 31 (**8**): 084101. DOI: 10.1088/1674-1056/ac6166

Goos-Hänchen and Imbert-Fedorov shifts in tilted Weyl semimetals

Shuo-Qing Liu(刘硕卿), Yi-Fei Song(宋益飞), Ting Wan(万婷), You-Gang Ke(柯友刚), and Zhao-Ming Luo(罗朝明)
Chin. Phys. B, 2022, 31 (**7**): 074101. DOI: 10.1088/1674-1056/ac4e03

A multi-frequency circularly polarized metasurface antenna array based on quarter-mode substrate integrated waveguide for sub-6 applications

Hao Bai(白昊), Guang-Ming Wang(王光明), Xiao-Jun Zou(邹晓鋆), Peng Xie(谢鹏), and Yi-Ping Shi(石一平)
Chin. Phys. B, 2022, 31 (**5**): 054102. DOI: 10.1088/1674-1056/ac373b

---

Design of an optically-transparent ultra-broadband microwave absorber

Mian Gao(高冕), Qiang Chen(陈强), Yue-Jun Zheng(郑月军), Fang Yuan(袁方), Zhan-Shan Sun(孙占山), and Yun-Qi Fu(付云起)†

College of Electronic Science and Technology, National University of Defense Technology, Changsha 410073, *China*

(Received 11 August 2022; revised manuscript received 9 October 2022; accepted manuscript online 14 October 2022)

The optical window of low-observable platform needs to be compatible with ultra-broadband absorption, hence an optically-transparent absorber with ultra-broadband absorption is designed and analyzed in this paper. The transparent materials indium-tin-oxide (ITO) film and polymethylmethacrylate (PMMA) are selected as the lossy layer and the supporting dielectric layer, respectively. The optically-transparent ultra-broadband absorber (OT-UBA) is composed of three layers of ITO square patterns, three layers of PMMA dielectric and a uniform ITO plane. The ITO square patterns can realize arbitrary equivalent series of RC (resistor and capacitor) circuit, so that three layers of ITO square patterns together with the ITO plane can achieve ultra-broadband absorption based on the equivalent circuit optimization. Measured results shows that the 90%-absorption bandwidth covers 2–17 GHz while the light transmittance achieves 59.6% with a total thickness of only 12.9 mm.

Keywords: ultra-broadband absorbers, optically-transparent, equivalent circuit optimization

PACS: 41.20.Jb, 42.25.Bs, 12.20.Fv **DOI:** 10.1088/1674-1056/ac9a39

1. Introduction

The cockpit of the low-detectable aircraft, the glass window of the ground vehicle instrument in the military field and the signal-shielding microwave technology room in the civilian field require a visible light-transparent absorber to meet the engineering needs of radar cross section (RCS) reduction and electromagnetic radiation resistance, also high light transmittance to provide the operator with clear vision. Existing literature research on transparent absorbers, in which indium tin oxide (ITO),[1] graphene,[2] metal grids[3] and other materials[4,5] are used as loss layers. Not only the light-transmitting properties, but also the electrical conductivity of the material should be considered in the impedance-matching problem. Therefore, it is difficult to design ultra-broadband absorbers under the constraints of high light transmission.

Metamaterials are artificially manufactured materials that do not exist in nature and have special performance advantages, such as electromagnetic regulation[6] and negative refractive index.[7] Metamaterials change some common properties of light and electromagnetic waves because the microstructure design of the metamaterial is smaller than the wavelength of action of the material.[8–12] It has great advantages in the design of broadband absorbers, the realization of broadband impedance matching, the miniaturization of absorbing structures, the realization of light and thin characteristics, and the use of indium tin oxide, graphene, and other materials to achieve microwave absorption and visible light transparency. There are many ways to realize ultra-broadband absorbers. On the one hand, optimizing the pattern of the structural unit and loading the lumped elements generates multi-resonance to expand the bandwidth. A resistive square loop was used in Ref. [13] as the unit cell of a wide-band absorber and the theoretical bandwidth realized was 112% with a thickness of $0.104\lambda_{\mathrm{L}}$. A double square loop with resistors of a single layer absorber was proposed to produce three resonances, which extended the fractional bandwidth to 126.8% for at least a 10 dB reflectivity reduction under normal incidence.[14] Various unit shapes such as the square patch,[15] cross,[16] gear-shape,[17] and bow-tie shape[18] were also tested. On the other hand, an effective way to expand the bandwidth is to stack multiple layers of dielectrics and lossy structure. The superimposed structure of multi-layer dielectric films has been proved to effectively expand the bandwidth, and the single lossy layer structure of the absorber can easily exceed the fractional bandwidth of 120%.[11,17,19] A three-layer slotted square loop structure is proposed to achieve a fractional absorption bandwidth of 150%.[20]

In this paper, a method for an ultra-broadband absorber characterized by its optically transparent property based on circuit optimization is proposed. The objective function can be realized by optimizing the circuit model, and the circuit model is designed into a wave-absorbing structure through the impedance law. The model of a resistive square patch was taken as an example, the light transmittance is considered and optimized in the design of the absorber, and an ultra-broadband transparent absorber is to testify the correctness of the method. Finally, this work extends the bandwidth to 157% on the constraint of 60% transmittance.

†Corresponding author. E-mail: yunqifu@nudt.edu.cn

© 2023 Chinese Physical Society and IOP Publishing Ltd

2. Materials and method

2.1. Selection of the transparent materials for the OT-UBA

ITO is a transparent conductive oxide material with good electrical conductivity, and resistivity can be as low as 10^{-4} Ω·cm. We measured the light transmittance of the ITO coated onto 0.125 mm PET film with different square resistance values. The square resistance of the ITO is determined by the thickness, which in turn affects the light transmittance. For example, when the thickness of ITO with a square resistance of 1 Ω/□ is 1000 nm, its light transmittance fluctuates greatly since the light transmittance is lower than 70% in most visible wavelengths. While the thickness of the square resistance of 10 Ω/□ is one-tenth of 1 Ω/□, the transmittance is increased to 80%, as shown in Fig. 1. The light transmittance can be improved (when designing a transparent absorber) by selecting an ITO with a larger square resistance.

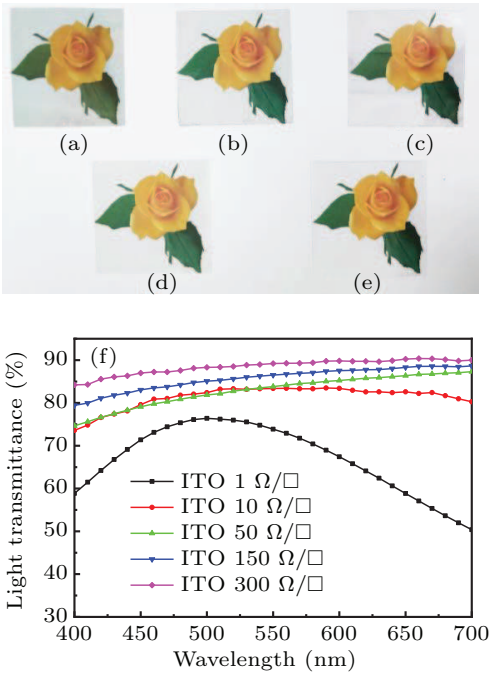


Fig. 1. Photos of ITO film with different square resistances. (a) R_s = 1 Ω/□, (b) R_s = 10 Ω/□, (c) R_s = 50 Ω/□, (d) R_s = 150 Ω/□, (e) R_s = 300 Ω/□. (f) the measured light transmittance of ITO at different thicknesses.

The dielectric material supporting the lossy layer also needs to be highly transparent. We compared the optoelectronic properties of some common transparent media, among which PMMA has the best light transmittance and the dielectric constant of 2.25, which is a good dielectric material. And it has the advantages of low price and easy processing. In addition, changing the thickness of the PMMA has little effect on the transmittance, so when optimizing the structure, the thickness of the medium can be used as the optimization object to only consider the absorbing factor.

2.2. Circuit simulation optimization

When the electromagnetic wave irradiates the surface of the absorber, it will be reflected, transmitted or absorbed by the absorber: $R^2 + T^2 + A^2 = 1$ (R, T, A represent reflectivity, transmissivity and absorptivity, respectively). Increasing absorptivity must simultaneously achieve small reflectivity and transmissivity. A small transmissivity can be used as a grounding layer through a small resistance to shield the electromagnetic waves. To reduce the reflection of electromagnetic waves, it is necessary to achieve impedance matching between the input impedance of the wave absorbing structure and the wave impedance of the air in a broadband range.

$$R = \left| \frac{Z_{\text{in}} - Z_0}{Z_{\text{in}} + Z_0} \right|, \tag{1}$$

where Z_{in} and Z_0 represent the input impedance of the absorber and the wave impedance of the air, respectively. According to transmission line theory, the dielectric material can be equivalent to the transmission line, and the resistive film layers can equal the impedance in parallel with the transmission line. Therefore, the input impedance of the absorbing structure can be designed and optimized by the equivalent circuit method to design broadband absorbers. An objective equation can be designed in advance and then the circuit parameters can be optimized. The parameter optimization process is a gradient optimization algorithm, which is calculated inside the circuit simulation software.

We assume absorption rate over 90, which covers the range 2–18 GHz as the objective function. A triple-layer absorber is selected because increasing the number of lossy layers can expand the bandwidth. Meanwhile, PET with a thickness of 0.12 mm is selected as the carrier for ITO, and the series *RC* circuit is selected as the lossy layers to invert the structure. The circuit model is shown in Fig. 2. The characteristic impedance of a transmission line is determined by the permittivity of the material, $Z_{c1} = 217.66$ Ω, $Z_{c2} = 251.33$ Ω, where $h = 0.125$ mm is the thickness of the PET. The uniform plane material as a reflective layer is also ITO, there is a resistor rather than an ideal conductor in the circuit model. The rest of the parameters are optimized by ADS software. Finally, we get the value of the circuit components in Fig. 2 and the reflectance curve in Fig. 5(a).

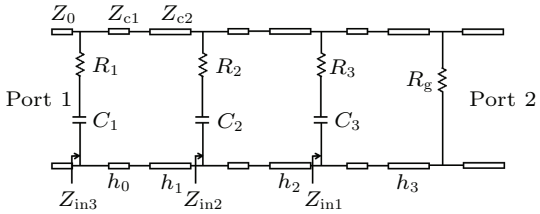


Fig. 2. The circuit model of the OT-UBA structure. Circuit parameters: R_1 = 200 Ω, C_1 = 25.12 fF, R_2 = 323 Ω, C_2 = 207 fF, R_3 = 136 Ω, C_3 = 673.5 fF, h_0 = 0.125 mm, h_1 = 2.8 mm, h_2 and h_3 both are 4.8 mm, R_g = 1 Ω.

As shown in Fig. 2, the input impedance per reference plane of the transmission line with any load impedance is

$$Z_{\mathrm{in}i} = Z_i \parallel \left(Z_{\mathrm{c}} \frac{Z_{\mathrm{in}(i-1)} + \mathrm{j}Z_{\mathrm{c}} \tan \beta l}{Z_{\mathrm{c}} + \mathrm{j}Z_{\mathrm{in}(i-1)} \tan \beta l} \right), \quad (i = 1,2,3), \tag{2}$$

where l is the length of the transmission line and β is the propagation constant. It is easy to conclude that when the $\mathrm{Real}(Z_{\mathrm{in}}) = 377\ \Omega$ as well as $\mathrm{Imag}(Z_{\mathrm{in}}) = 0$, the input impedance is perfectly matched with air according to Eq. (1). The input impedance of each layer to the ground and their corresponding reflection coefficient are calculated as shown in Fig. 3. With the increase to three in the number of lossy layers, the real part of the impedance is close to 300 Ω, and the imaginary part is kept near 0 Ω. The input impedance is getting closer to the air impedance in the entire working frequency band, so the reflectivity is getting smaller, and the corresponding resonance points are increased to three, which is why it can achieve a good impedance matching in a wide frequency range.

According to Ref. [21], a series-connected RC circuit can be realized with a square patch structure. In order to realize the circuit parameters with the actual structure, the impedance law of resistive square patch is used. For any square patterns element with different R_{s} and structural parameters, its accurate equivalent surface impedance $Z = R + \mathrm{j}X$ can be extracted by full-wave simulation software such as CST and HFSS. The real part of the impedance is just the series equivalent resistance R, while the imaginary part X is determined by the capacitance C. Based on the extracted equivalent surface impedance by full-wave simulation software CST, the capacitance C can be calculated using curve-fitting methods. For example, for an element with $p = 5$ mm, $d/p = 0.85$ (d and p are the side length of the ITO square patterns and the period of the array, respectively) and $R_{\mathrm{s}} = 100\ \Omega/\square$, the calculated capacitance C is 40.3 fF, so that the imaginary X can be written as

$$X = -\frac{1}{\omega C}. \tag{3}$$

The equivalent capacitance value can be calculated from any frequency point on the impedance curve.

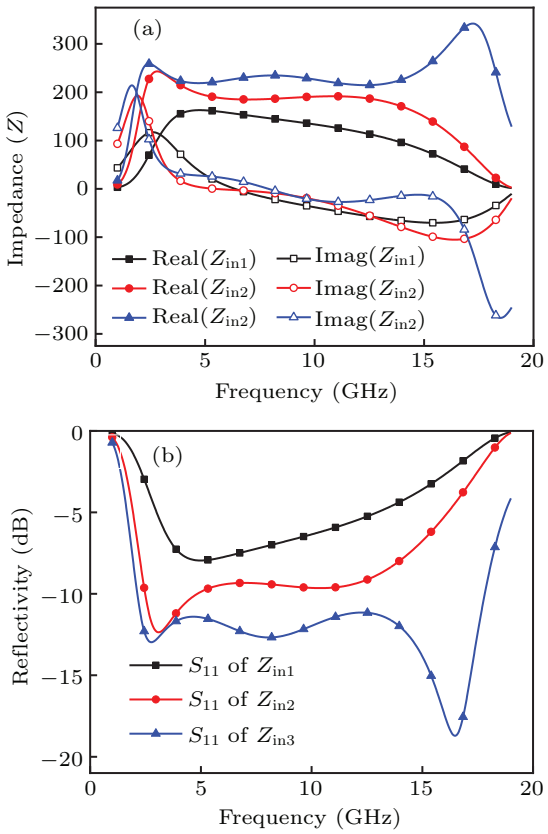


Fig. 3. (a) The input impedance of each layer to the ground and (b) their corresponding reflectivity.

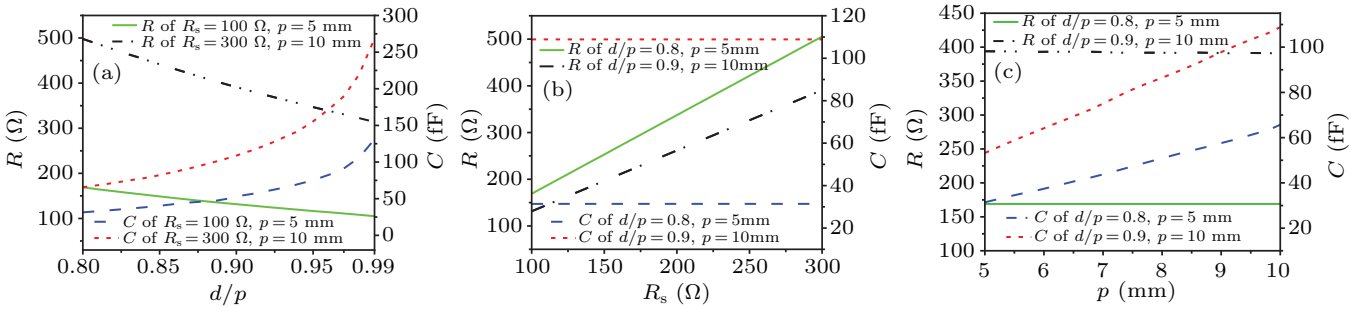


Fig. 4. The impedance law of ITO square pattern elements. (a) The variation of equivalent impedance with d/p, fixed R_{s} and p. (b) The variation of equivalent impedance with R_{s}, fixed d/p and p. (c) The variation of equivalent impedance with p, fixed R_{s} and d/p.

The impedance of ITO square pattern elements with different periodicity p (mm), patch size ratio d/p and square resistance R_{s} (unit: $\Omega/\square$) have been simulated and extracted using full-wave simulation CST software. To further study the variation law of ITO square pattern elements equivalent impedance and structure, and establish a mapping relation database, we fixed two of the three parameters p, R_{s} and d/p to study the effect of another parameter on impedance. Meanwhile, we calculated the equivalent resistance R and capacitance C under different structure sizes, in the form of control variables; the abscissa of each value is used to describe the variation law of RC parameters with other parameters, shown

in Fig. 4. The law of resistance R can be summarized as follows: (i) R changes linearly with a negative correlation to the patch ratio d/p. (ii) R changes strictly proportionally to the square resistance R_s. e.g., $d/p = 0.9$ and $p = 10$ mm, the ratio is $R = 1.3R_s$. (iii) R does not change with the periodicity p.

The law of capacitance C can be summarized as follows: (i) C increases exponentially with d/p, where $d/p = 1$ is the asymptote. (ii) C remains the same as the square resistance increases. (iii) C increases linearly with periodicity.

This means that the resistance and capacitance of the patch can be controlled by the square resistance and periodicity alone, respectively. Figure 3 shows the variation law of the corresponding parameters within a part of the range. The range shown in the figure, which is the same as the law in Fig. 3, can be analogized. In turn, we conclude that any RC circuit parameters can be realized by the ITO square pattern elements by tuning the periodicity, the patch size and the surface resistance. This is the foundation of the design of an ultra-broadband absorber through circuit optimization.

The idea of the design is briefly to first adjust the structure size to achieve the required value of the capacitance, and then adjust the square resistance of the patch to achieve the required equivalent resistance. The square patch structure realizes the optimized component parameters, the transmission line can be replaced with a medium with the same thickness and dielectric constant. Thus, the circuit model is designed as a complete absorbing structure model.

2.3. Structural design and analysis

The final parameters of the circuit and structure are shown in Table 1. The ITO structure arranged periodically in each layer is equivalent to the RC element in the circuit, the dielectric layer is equivalent to a transmission line, together with the overall structure which is shown in Fig. 5.

Table 1. Parameters of circuit models and ITO square pattern elements.

Parameters	Value	Parameters	Value
R_1	200 Ω	R_{s1}	70 Ω/□
R_2	323 Ω	R_{s2}	285 Ω/□
R_3	136 Ω	R_{s3}	130 Ω/□
C_1	25.1 fF	R_g	10 Ω/□
C_2	207 fF	d_1	3.1 mm
C_3	673.5 fF	d_2	4.8 mm
h	0.125 mm	d_3	9.9 mm
h_1	2.8 mm	p_1, p_2	5 mm
h_2, h_3	4.8 mm	p_3	10 mm

The reflectivity and absorptivity curves for circuit optimization and structural simulation comparisons are shown in Fig. 6(a). The bandwidth of the optimized circuit $S_{11} < -10$ dB (absorption rate is over 90%) is 218.7 GHz meets the requirements of the objective function and is basically consistent with the S_{11} curve simulated by the designed ITO square pattern elements-based absorber. The high similarity of the curves proves the accuracy of the design.

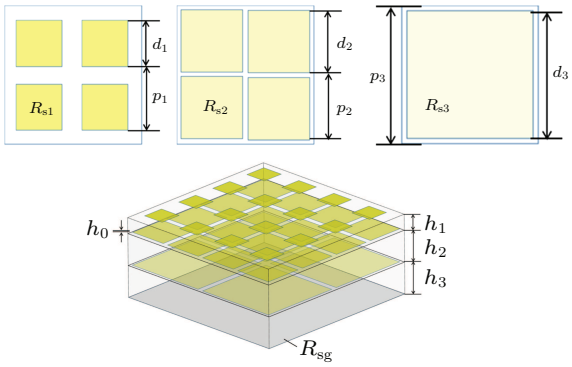


Fig. 5. The geometry of the OT-UBA structure.

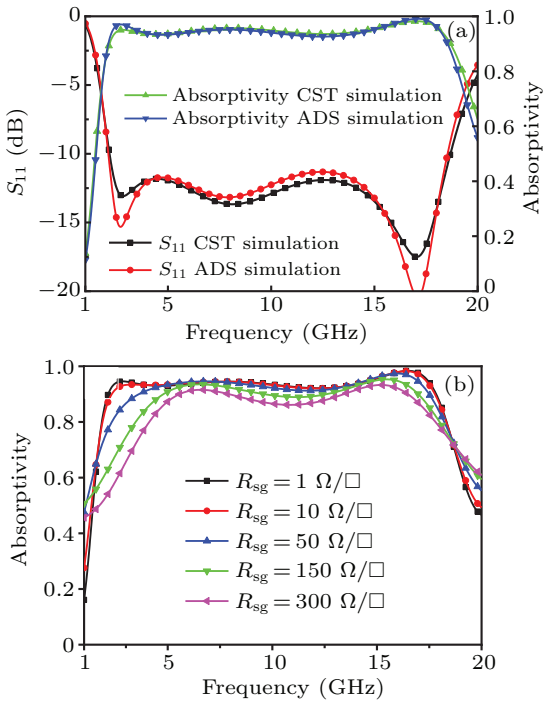


Fig. 6. (a) Circuit simulation in ADS and full-wave simulation in CST. (b) Simulated absorption under different square resistance R_{sg}.

The square resistance in the structure needs to be designed with a pre-determined value for impedance matching, which cannot be changed arbitrarily, and its light transmittance cannot be optimized. In comparison, the square resistance of the reflective layer can be adjusted to improve light transmittance without reducing absorption. We simulated the effect of R_{sg} on the absorption from 1 Ω/□ to 300 Ω/□, as shown in Fig. 6(b). The high-frequency component is almost unchanged, while for the low-frequency part, the reflectivity gradually increases so that it results in a narrowing of the absorption bandwidth as the square resistance increases. However, the thickness decreases by 900 nm when the square resistance increases from 1 Ω/□ to 10 Ω/□. When the square

resistance exceeds 10 Ω/□, the thickness is only reduced by tens of nanometers; the influence of light transmittance becomes very tiny. Therefore, it is more appropriate to use a square resistance of 10 Ω/□ to comprehensively consider the influence of the square resistance on the microwave absorptivity and light transmittance.

It is certainly important to study the absorption performance of the designed absorber under oblique incidences. Simulated absorptivity performance of the designed absorber for both TE and TM polarizations under oblique incidence are shown in Fig. 7. The figure shows the absorption is acceptable up to $\theta = 30^\circ$ for TE polarization. For TM polarization, the absorption effect is better as the incident angle increases. The performance of oblique incidence is related to the period of the unit. It is necessary to consider oblique incidence in both design and engineering applications.

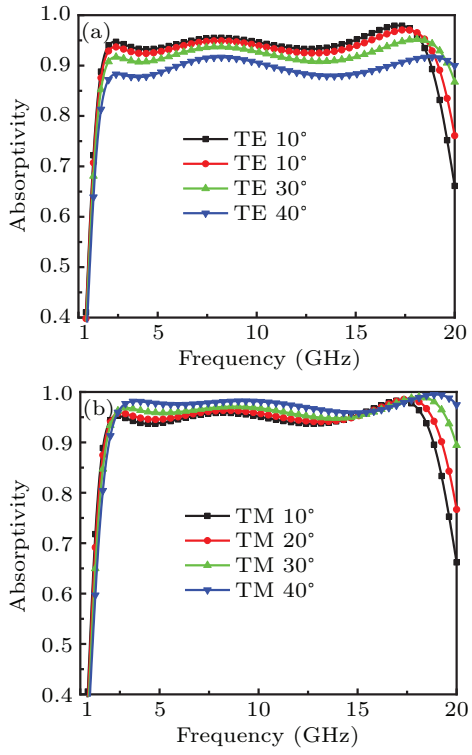


Fig. 7. Simulated absorptivity under different oblique incidence angles for (a) TE and (b) TM polarization.

The design method in this paper is guided by the objective function, a strict mapping relationship between structural parameters and circuit parameters is established. For the ultra-wideband frequency response obtained by any circuit optimization, the circuit parameters can be realized by the corresponding structural parameters obtained from the mapping relationship. In addition, this method can more clearly understand the principle of wave absorption by means of the equivalent circuit method, as when the actual demand changes, the objective function can be redesigned, and the absorbing structure can be designed efficiently.

3. Fabrication and measurement

We plated ITO with different square resistances on a 0.125 mm PET film with corresponding square patterns and then glued the PET and PMMA with optically clear adhesive (OCA). The composition of the OCA is PET material, and the influence of the thickness of 10 μm on the wave absorption can be ignored. The sample size is 300 mm×300 mm and contains 900 periodic units, as shown in Fig. 8. frequency shift occurs for the resonant frequencies and the absorptivity is less than the simulation in some frequency bands through the comparison of simulation and measurement curve. The errors between them are the tolerances introduced during fabrication, such as the square resistance of the ITO, and their values are within range (R_{s1} in 130–150 Ω/□, R_{s2} in 280–300 Ω/□, R_{s3} in 70–80 Ω/□) and the square resistance of each unit is not fixed at the same value through measurement. Errors are caused by uneven tiny air bubbles when pasting between sheet materials. In addition, the uncertainty of the permittivity and the thickness of the dielectric material and the uncertainty in the measurement process can also lead to error. Despite the above errors, the absorption bandwidth obtained by the test can reach 2–17 GHz. Thus, we conclude that the simulations shown in Fig. 9(a) are convincing and valid.



Fig. 8. Photo of the fabricated OT-UBA structure.

The light transmittance of the OT-UBA structure with different R_{sg} was measured by a haze meter. The results are presented in Fig. 9(b). When the square resistance of the reflective layer is 1 Ω/□, the light transmittance of the whole structure is less than 50%. The transmittance drops sharply after the 550 nm band, which is the same as the measured transmittance of 1 Ω/□ single-layer ITO, which proves that the transmittance of the reflective layer has a great influence on the transmittance of the overall structure. When the square resistance of the reflective layer is 10 Ω/□, the light transmittance increase to 59.6%. Increasing the square resistance of the reflective layer improves the overall light transmittance of the structure without reducing absorption, which is consistent with the previous conclusion.

We have also measured the oblique incidence, which is basically consistent with the law shown in the simulation. The results show that a good absorbing effect in the range of 40° can be reached. For a 40° TM-polarized wave, the absorbing body showed better performance. Under the condition that the absorption frequency of the low-frequency part remains unchanged, the high-frequency part extends to more than 18 GHz, and the absorptivity in the entire frequency band is above 80%, as shown in Fig. 10.

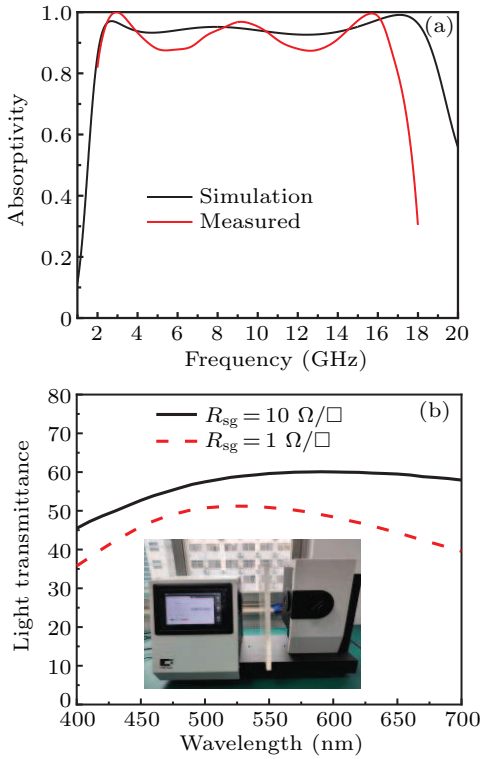


Fig. 9. (a) Simulated and measured absorptivity of the sample at normal incidence. (b) The optical light transmittance of the total OT-UBA structure with different R_{sg}.

To better understand the performance of our designed OT-UBA structure compared to existing transparent absorbers reported in the literature, we list the bandwidth and light transmittance performances in Table 2 for some of the existing transparent absorbers, including the one presented in this paper. Obviously, it is difficult to balance the absorption bandwidth and light transmittance very well. The data shows that the absorption bandwidth of our OT-UBA structure has an absolute advantage with almost the same relative thickness. The literature[19,22,23] pays more attention to the light transmittance and does not obtain a wider absorption bandwidth. Compared to bandwidth-conscious work,[17,24] our work extends the absorption bandwidth to 157% at a transmittance level of 60%. In this work, the absorption bandwidth and transmittance are comprehensively considered, and the absorption bandwidth is effectively expanded on the premise of maintaining the transmittance, which is of great significance in practical applications and provides a reference idea for studying the ultra-wideband wave absorber under the constraint of optical transparency.

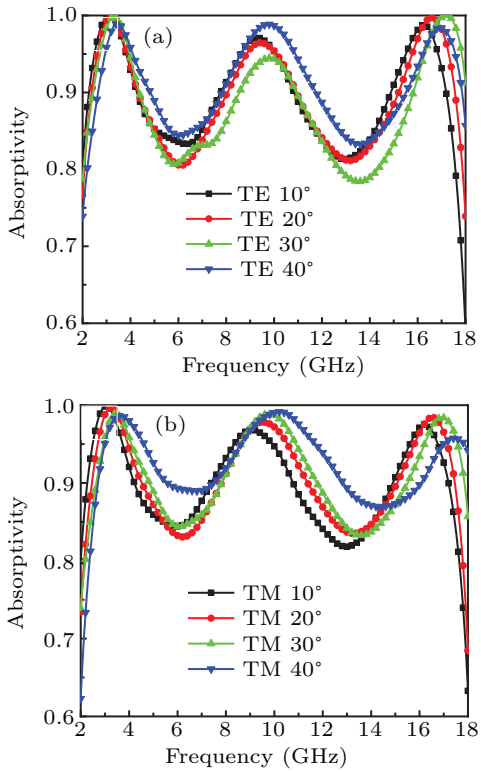


Fig. 10. Measured absorptivity of the sample at the different incidences for (a) TE and (b) TM polarization.

Table 2. Bandwidth, thickness and light transmittance comparison of absorbers.

Ref.	Bandwidth (GHz, %)	Thickness (unit: λ_L)	Light transmittance (%)	Lossy layers
[22]	4.3–11.1 (88.3)	9.7 mm, 0.138	69.4	2
[23]	6–16.7 (94.3)	4.42 mm, 0.088	85.7	2
[19]	6.1–18.4 (101.6)	4.2 mm, 0.086	86	3
[17]	3.86–15 (118.1)	6.1 mm, 0.083	53	1
[24]	4.3–18.7 (125.2)	6 mm, 0.086	65	1
This work	2–17 (157.9)	12.9 mm, 0.086	59.6	3

4. Conclusion

In this paper, an ultra-broadband design method based on transparent materials is proposed. The total thickness of the ultra-broadband absorber is 12.9 mm, which is only $0.086\lambda_L$ at the lowest operating frequency of the absorber. A prototype was fabricated and measured, proving the accuracy of the design. Compared with the existing literature, the OT-UBA has a wider absorption bandwidth under the condition of 60%

light transmission. In future work, we will try to improve the overall light transmittance under the condition of meeting the absorption bandwidth. In addition, in practical engineering applications, even if parameters such as materials and circuit structures are limited, the structure can be quickly and accurately designed according to requirements, which has a significant application value.

Acknowledgements

Project supported by the National Natural Science Foundation of China (Grant Nos. 61901492 and 61901493) and Provincial Natural Science Foundation of Hunan (Grant No. 2022JJ30665).

References

[1] Xiao H, Qin R, Lv M and Wang C 2020 *Appl. Sci.* **10** 9125
[2] Yi D, Wei X and Xu Y 2017 *IEEE Trans. Nano* **16** 484
[3] Wei L and Atif S 2019 13*th European Conference on Antennas and Propagation (EuCAP)*, 31 March 2019–05 April 2019, Krakow, Poland
[4] Wang Q, Bi K and Lim S 2020 *IEEE Access* **8** 175998
[5] Lu F and Han T 2019 *Photonics & Electromagnetics Research Symposium - Fall (PIERS - Fall*, 17–20 December 2019, Xiamen, China
[6] Wang B L 2020 *Chin. Phys. B* **29** 045202
[7] Hong G, Shun Z, Xiao W and Xin L 2017 *Chin. Phys. Lett.* **34** 25
[8] Wang F and Wei B 2019 *Acta Phys. Sin.* **68** 244101 (in Chinese)
[9] Hai L, Yang L and Bin W 2015 *Chin. Phys. Lett.* **32** 44102
[10] Wei C, Hong L and Min S 2016 *Chin. Phys. Lett.* **33** 124101
[11] Tao Z and Hou Z 2020 *Chin. Phys. B* **29** 094101
[12] Zhi S, Meng Y and Bi X 2020 *Chin. Phys. B* **29** 104101
[13] Costa F, Monorchio A and Manara G 2010 *IEEE Trans. Antennas. Propag.* **58** 1551
[14] Shang Y, Shen Z and Xiao S 2013 *IEEE Trans. Antennas. Propag.* **61** 6022
[15] Li L, Xi R, Liu H and Lv Z 2018 *Appl. Phys. Express* **11** 52001
[16] Sheokand H, Singh G, Ghosh S, Saikia M, Srivastava K V, Ramkumar J and Ramakrishna S A 2018 *Twenty Fourth National Conference on Communications NCC*, 25–28 February 2018, Hyderabad, India, pp. 113–117
[17] Zhang L, Shi Y, Yang J X, Zhang X and Li L 2019 *IEEE Access* **7** 137848
[18] Jang T, Youn H, Shin Y J and Guo L J 2014 *ACS Phot.* **1** 279
[19] Sheokand H, Singh G, Ghosh S, Ramkumar J, Ramakrishna S A and Srivastava K V 2019 *IEEE Antennas Wireless Propag. Lett* **18** 113
[20] Sun J, Liu L, Dong G and Zhou J 2011 *Opt. Express* **19** 21155
[21] Alireza K and Anders K 2009 *IEEE Trans. Antennas. Propag.* **57** 2307
[22] Jiang H, Yang W, Li R, Lei S, Chen B, Hu H and Zhao Z 2021 *IEEE Antennas Wireless Propag. Lett* **20** 1399
[23] Xiao H, Qin R, Lv M and Wang C 2020 *Appl. Sci.* **10** 9125
[24] Min P, Song Z, Yang L, Dai B and Zhu J 2020 *Opt. Express* **28** 19518